

Classification and reconstruction of images in the problem single-pixel imaging using classical and quantum neural networks

Sofya Manko and Dmitriy Frolovtssev

Department of General Physics and Wave Processes, Lomonosov Moscow State University, Moscow, Russia.

*Corresponding author(s). E-mail(s): manko.sd17@physics.msu.ru;
Contributing authors: frolovcev.dmitriy@physics.msu.ru;

Abstract

Single-pixel cameras can be an excellent solution for light ranges outside the visible spectrum, combined with machine learning, they can analyze images quickly enough for practical applications. In the future of the development of quantum technologies, quantum computers can further speed up the solution of such problems. In this work we simulated a single-pixel detection experiment using Hadamard basis patterns, where images from the MNIST handwritten digit dataset were used as objects. There were selected 64 measurements with maximum variance (6% of the number of pixels in the image). We created algorithms for classifying and reconstruction images based on these measurements using classical fully connected neural networks and parameterized quantum circuits. Classical and quantum classifiers showed accuracies of 96% and 95% respectively after 6 training epochs, which is quite competitive result. Image reconstruction was also demonstrated using classical and quantum neural networks after 10 training epochs, the structural similarity index values were 0.76 and 0.25, respectively, which indicates that the problem in such a formulation turned out to be too difficult for quantum neural networks in such a configuration for now.

Keywords: Quantum machine learning, Parameterized quantum circuits, Single-pixel imaging, Compressive sensing, Image classification, Image reconstruction

1 Introduction

In single-pixel detection [1], the light intensity scattered by an object is measured by a single photodetector (not matrix as in usual case). Illuminating an object with structured light with a certain set of masks (patterns) allows us to reconstruct an image from such measurements, so that we can obtain spatial resolution without having it in the detector itself. The image is reconstructed

by solving the inverse problem, knowing the measurement and pattern at which it was obtained. The single-pixel detection method makes it possible to obtain images at wavelengths outside the visible light range (where is no cheap imaging method, as CCD camera in the visible range), with precise time or depth resolution, and also in turbid environments, which causes greater practical significance of the direction.

Quantum machine learning (QML) is a promising science direction [2–5], located at the intersection of quantum physics and computer science, in which machine learning methods are developed and studied that can effectively use the unique features of a quantum computer such as superposition and entanglement [6]. In addition, the variational (parameterized) quantum circuits used in quantum machine learning are resistant to the noise of quantum processors [7, 8], which means they can potentially find their useful application before other known quantum algorithms, which require a fault-tolerant quantum computer. Quantum computing is developing to solve various problems in such fields as logistics, finance, medicine and machine learning [9–13]. This work is aimed at developing this approach as applied to the problem of single-pixel image detection and compare it’s results with classical neural networks (NN), that have shown good results in this area in recent years.

Due to the fact that quantum processors currently have a small qubit register size and the simulation has exponential complexity depending on the number of qubits, this work uses quite primitive dataset and compares with classical models with simple architecture.

2 Related work

Single-pixel detection is a promising and cost-effective imaging technique at wavelengths throughout the electromagnetic range (i. g. X-ray [14–16], terahertz [17–19]). Single-pixel detection is often used in the near-infrared range due to the availability of detectors with good sensitivity and sources operating in this range. This wavelength range is particularly suitable for detection through scattering media such as fog [20, 21], and has also been used to detect and visualize methane leaks [22].

For practical using of single-pixel imaging systems, it is needed to significantly reduce the number of patterns and measurements required to increase the speed of this approach. It was demonstrated that redundancy in the structure of most natural signals or images can be used for this purpose, images are sparse in an appropriate basis, that means that they have many coefficients close to or equal to zero [23, 24].

It is also worth noting that many problems does not require reconstruction of the complete signal, this is the case in applications such as detection or classification [25].

Recently, works on single-pixel imaging using machine learning methods has begun to appear. For example, in [26], using neural networks (NN), a set of patterns that were most effective for an object was constructed, and compression of a set of masks up to 4% was demonstrated to reconstruct 2D images at video signal speed. This model was later used to obtain 3D images in [27]. And in [28], a neural network was used to develop a small number of patterns to classify and identify very fast moving objects. This means that single-pixel cameras with image processing using neural networks are an excellent candidate for many practical applications, such as controlling self-driving cars, night-vision, gas sensing and medical diagnostics. In addition, it is possible to use alternative types of computing such as optical machine learning for image reconstruction [29].

Quantum machine learning is a rapidly evolving field and has the potential to revolutionize various areas of computing and achieved a number of great results. The work [30] demonstrated the outperforming of a quantum neural network over a classical one in classifying the Earth Observation dataset (EuroSat) by more than 1% of accuracy. In [31] Quantum neural networks (QNN) was applied to various datasets using the single-shot training scheme, which allows input samples to be trained in a N-level quantum system, it has exceed a classical NN with zero hidden layer. However, when two more hidden layers were added to architecture, the classical NN surpassed the QNN.

Quantum neural networks, like classical ones, have a number of problems, such as a barren plateau that decreases the gradient as the number of qubits increases [32, 33], quantum convolutional neural networks (QCNNs) help to cope with this problem [34]. QCNN has achieved excellent classification accuracy despite having a small number of free parameters, noticeably better than CNN models under the similar training conditions [35]. Recent studies have also explored hybrid quantum–classical convolutional neural networks (containing classical and quantum layers) and demonstrated the classification of images outperforming classical CNNs [36–38]. The concept of quantum

generative adversarial networks for image generation was implemented experimentally (using real quantum setup) [39, 40].

Thus, by introducing quantum machine learning into a single-pixel imaging task, promising results can be obtained.

3 Data

A simple method of obtain an image using a single-pixel detector is to measure each pixel in turn (raster scanning). However, sequentially measuring information about only one pixel in turn is an inefficient use of light capabilities. More common scanning strategy is to use a sequence of spatially resolved light patterns and measure the intensity as different patterns illuminate the object. To reduce the number of measurements required for high quality image restoion a set of orthogonal patterns are used, such as the Hadamard basis.

In this work, a vector of numbers obtained by simulating single-pixel measurements is used as data, a set of Hadamard matrices is used as patterns, and a dataset of images of handwritten digits MNIST (28×28) is used as objects, containing objects of ten classes, images of numbers (from 0 to 9). The dataset consists of a training set of 60 000 images and a test set of 10 000 images.

Matrix O of size $n \times n$ is our object which we want to reconstruct, and M is a vector of obtained measurements of length n^2 . In order to measure the desired object in the Hadamard basis, we need a set of n^2 different Hadamard patterns $H_n^{(i)}$ (Fig. 1), which can be represented as a matrix:

$$H_2 = \begin{pmatrix} 1 & 1 \\ 1 & -1 \end{pmatrix}, \quad (1)$$

$$H_{2^k} = \begin{pmatrix} H_{2^{k-1}} & H_{2^{k-1}} \\ H_{2^{k-1}} & -H_{2^{k-1}} \end{pmatrix} = H_2 \otimes H_{2^{k-1}},$$

where $2^k = n$ - number of width and high pixels of the image (object).

Note that $H_n = H_n^{-1} = H_n^T$, which means that image reconstruction can be performed without matrix inversion.

The i -th measurement in the Hadamard basis can be represented as a scalar product $M_i = H_n^{(i)} * O$, with the pattern and object extended into vectors (row and column, respectively), and



Fig. 1: Example of several Hadamard patterns $H_n^{(i)}$ (rows of matrix H_n resized to $n \times n$)

the inverse problem of image reconstruction, can be represented as $O = \sum_i H_n^{(i)} \times M_i$.

In order to be able to convolve the image with the Hadamard matrix, the dimensions of which are $\propto 2^k$, the size of the images was changed to (32×32) . Thus, for each object, a measurement vector M of length 1024 ($32 \cdot 32$) elements can be calculated.

But in reality, taking so many measurements (responses to the different light patterns), which are also redundant (since images of objects are usually quite sparse), takes a long time, and their reconstruction is computationally difficult, especially for high-resolution images (with a large number of pixels). However, cameras must capture images at high speed. Therefore, we need to reduce the number of required measurements and leave only the most significant ones for our objects.

Using classical neural networks, which would be described in section 4.1, we investigated the dependence of the training quality on the number of measurements with the biggest variance through the dataset (most significant) in the input layer of the neural network, it is shown in Fig. 2. Based on the obtained results, we decided to reduce the number of measurements to 64, which is approximately 6% of the total number of measurements, making the problem of image reconstruction to become underdetermined (the number of variables is greater than the number of equations) and one of the ways to solve this problem is neural networks.

4 Methods

In this paragraph we will go into details of architectures both classical and quantum neural networks for classification and image reconstruction.

4.1 Classical neural networks

For the classic solution, fully connected neural networks were used with $ReLU(x) = \max(0, x)$ as

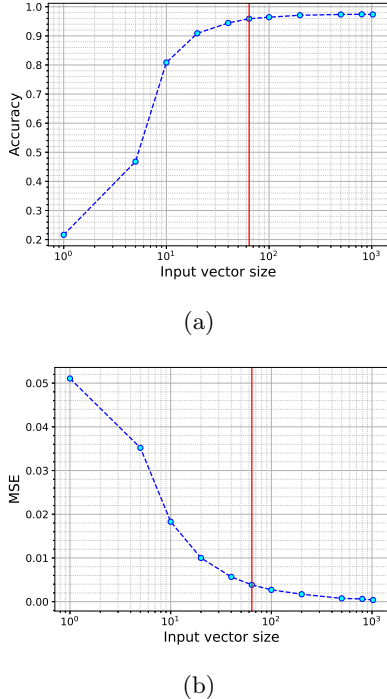


Fig. 2: Dependence of test set (a) - accuracy of classification, (b) - mean squared error of image reconstruction, - on the number of measurements in the Hadamard basis in the input layer of neural network

activation function and Adam as optimizer. The metrics used in this work are Cross-Entropy (Eq. 2) loss for classification problem and MSE (Eq. 3) for the regression problem of image reconstruction. The architecture of the classifier consists of one hidden layer ($64 \rightarrow 128 \rightarrow 10$ neurons for *input* \rightarrow *hidden* \rightarrow *output* layers respectively, that is, 9 610 trainable parameters (according to the Eq. 4)). To reconstruct images, a neural network of four hidden layers is used ($64 \rightarrow 1\ 000 \rightarrow 2\ 000 \rightarrow 4000 \rightarrow 2000 \rightarrow 1024$ neurons, that is, 20 122 024 trainable parameters (Eq. 4)).

Cross-entropy is given by the following expression:

$$L = -\frac{1}{N} \sum_{i=1}^N \sum_{j=1}^M p_{i,j} \log_2 q_{i,j}, \quad (2)$$

where i is the number of the element in the batch, N - their number in the batch, j - class number, M - number of classes ($M = 10$), p_i - true probability distribution by class for the i -th batch (zero for

all classes except the true one under number j_{true} , for which $p_{i,j_{true}} = 1$) q_i - predicted probability distribution by class for the i -th batch, that is, $q_{3,7}$ is the probability predicted by the neural network with which the 3rd element of the batch belongs to the 7th class (that is, the number “7”).

Mean squared error loss functions can be written as follows:

$$L = \frac{1}{N} \sum_{i=1}^N \sum_{j=1}^M (y_{i,j} - f_j(x_i))^2, \quad (3)$$

where i is the number of the element in the batch, N - their number in the batch, j - pixel number, M - number of pixels (in our case $M = 1024$), $y_{i,j}$ - true value of the j -th pixel in the i -th batch, $f_j(x_i)$ is the value of the j -th pixel predicted by the model that received a vector of values in the Hadamard basis x_i as input.

The expression for calculating the number of parameters of a neural network:

$$\sum_{i=1}^m (n_{out}^{(i)} \cdot (n_{in}^{(i)} + 1)), \quad (4)$$

where m is number of layers, $n_{in}^{(i)}$ - number of elements at the input of the i -th layer, $n_{out}^{(i)}$ - number of elements at the output of the i -th layer.

4.2 Quantum neural networks

Quantum neural networks operate with qubits - quantum bits of information. Qubit can be described by a state vector $|\psi\rangle = \cos \frac{\theta}{2} |0\rangle + e^{i\phi} \sin \frac{\theta}{2} |1\rangle = \begin{pmatrix} \cos \frac{\theta}{2} \\ e^{i\phi} \sin \frac{\theta}{2} \end{pmatrix}$, where θ, ϕ are angles on a Bloch sphere [6].

To train quantum neural networks parameterized quantum circuits with classical optimizer feedback loop are used. Variational quantum circuit is a sequence of quantum gates depending on tunable parameters (rotation operator as in Eq. 6) and entangling gates, which connects qubits and responsible for nonlinearity (like activation function in classic) and “neurons” connection.

For quantum solution parameterized quantum circuits were used with Adam optimizer. For quantum classification problem we used Margin loss (Eq. 5 due to the architectural feature) and MSE (Eq. 3) for image reconstruction.

Margin loss can be described by the formula:

$$L_i = \sum_{j=1}^N \sum_{j \neq y}^M \max(0, s_j - s_{y_i} + \Delta), \quad (5)$$

where i is the number of the element in the batch, N - their number in the batch, j - class number, M - number of classes ($M = 10$), s_j - the result of the prediction of the j -th classifier from the input data x_j , lying in the interval $[-1, 1]$, s_{y_i} - true class label for x_j , and Δ is a hyperparameter called margin (we set $\Delta = 0.15$)

Consider how a quantum neural network works.

At first we need to encode classical data to qubits, which could be done by the procedure called amplitude embedding so that we prepare our qubits in state $|\psi_x\rangle = \sum_{i=1}^{64} x_i |i\rangle$, where quantum state complex amplitudes become equals to normalized classical feature values, that allows us to encode features to $\log_2 n_{feat}$ qubits. It is worth clarifying that this method of data encoding as amplitude embedding is not optimal for near-term hardware installations, since it has a depth that grows exponentially with the number of qubits, but is acceptable for simulation, since it requires a significantly smaller number of qubits than other encoding methods, which is very important for classical simulation. Research into how to most efficiently encode classical data into qubits is now actively underway in the global community [41].

Next we operate qubits state with parameterized circuit, consisting of layers called ansatz (represented in Fig. 3). A quantum circuit contains several successive layers, after that we have a quantum state depending on the parameters. We can somehow measure the qubits and, using the results obtained, adjust the parameters of the variational circuit using a classical optimizer.

Quantum real parameterized rotation gate R_Y and entangling gate $CNOT$ used in Fig. 3 can be written as matrices:

$$R_Y(\theta) = \begin{pmatrix} \cos(\frac{\theta}{2}) & -\sin(\frac{\theta}{2}) \\ \sin(\frac{\theta}{2}) & \cos(\frac{\theta}{2}) \end{pmatrix} \quad (6)$$

$$CNOT = \begin{pmatrix} 1 & 0 & 0 & 0 \\ 0 & 1 & 0 & 0 \\ 0 & 0 & 0 & 1 \\ 0 & 0 & 1 & 0 \end{pmatrix} \quad (7)$$

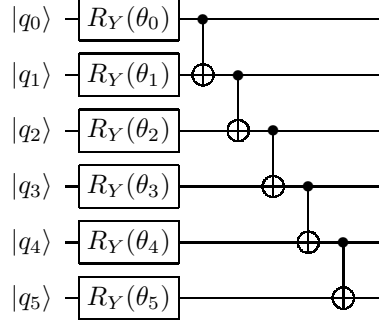


Fig. 3: One layer structure of parameterized quantum circuit

Now we can describe the architectures of quantum neural networks used in this work.

Classification circuit consists of 6 qubits ($\log_2 64$), highly entangled layers (how is shown in Fig 3 with different $n_{params} = n_{qubits} \cdot (n_{layers} + 1) \text{ angles} + 1 \text{ bias}$ trainable parameters ($n_{layers} + 1$ because usually after all layers is added an additional one without entangling gates) and one measurement of the expected value of the first qubit. This scheme is a binary classifier that determines the probability of our data belonging to one of the classes or to all others (it solves a binary problem, where 1 means belonging to this class, -1 to some other). Margin loss (from Eq. 5) allows us to train our networks using one-against-all strategy. So we have $n_{classes}$ different quantum circuits with their own parameters and training independently. In total this quantum classifier has $n_{classes} \cdot n_{params}$.

Then the number of parameters for quantum classification is following:

$$n_{classes} \cdot (n_{qubits} \cdot (n_{layers} + 1) + 1) \quad (8)$$

Quantum algorithm of single-pixel images reconstruction is quite similar to the one described above, but there is no need for different trainable circuits. Another difference is that to produce an image at the output of the circuit, we need 4 more qubits (thus $2^{(6+4)} = 1024 = 32 \cdot 32$), which are initially in state $|0\rangle$. So our ansatz from Fig. 3 need to be expanded to 10 qubits. In the end of the circuit we measure the probabilities of qubit system to be in each possible state (2^{10} numbers). This

quantum network has $n_{qubits} \cdot (n_{layers} + 1)$ angles as trainable parameters.

Due to the long training time using quantum simulator, we decided to use a small part of the MNIST dataset (640 images of zeros and 640 ones) for the reconstruction problem.

5 Results

The neural networks for image classification by 64 measurements in Hadamard basis presented in previous section were trained for 6 epochs. We tried quantum neural network with different number of layers and training results are shown in Fig. 4 and Table 1. It can be seen that as the number of trainable parameters of a quantum network increases, the final accuracy also raises. And when it is compared with the number of parameters of the classical network, it would exceed its accuracy according to the nature of the observed dependence [42].

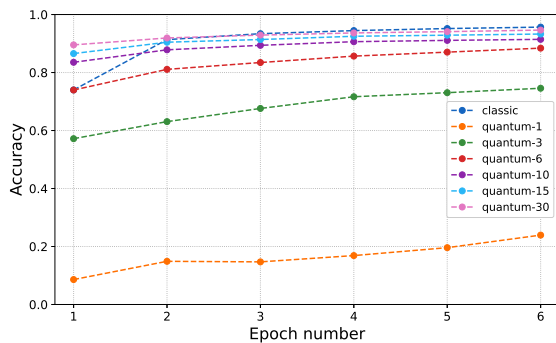


Fig. 4: Validation accuracy while training various classification neural networks, quantum with different number of layers (1, 3, 6, 10, 15, 30) and classical

Despite the seemingly small size of the problem, the training using quantum neural networks takes a significant amount of time, this is due to the fact that simulating quantum circuits using a classical computer is computationally complex and time-consuming [43]. It is obvious that quantum machine learning loses significantly in speed on small-scale problems due to the big setup overheads, however, with increasing scale, an advantage over classical networks is predicted [2-5].

Table 1: Different classification networks results

Network	$n_{parameters}^1$	Accuracy	Training time ²
classical	9 610	0.96	15.6 s
quantum-1	130	0.24	5.5 h
quantum-3	250	0.75	9.1 h
quantum-6	430	0.88	15.3 h
quantum-10	670	0.91	22.2 h
quantum-15	970	0.93	31.7 h
quantum-30	1 870	0.95	63.8 h

¹According to Eq. 4 and Eq. 8 for classical and quantum networks respectively

²Google Colab T4 GPU time for classical solution and PennyLane lightning.qubit simulator on Intel(R) Core(TM) i7-11700 workstation for quantum solution

The results of training networks to reconstruct images from simulated single-pixel detection experiment are presented in Fig. 5. As you can see the gap between the classical neural network and quantum ones with different numbers of layers is very large. The training time of a quantum neural network depends linearly on the number of layers in it. The dependence of the improvement in the quality of the reconstructed image with an increase in the number of layers does not allow us to hope for the ability to observe a comparable result for a quantum neural network within a reasonable simulation time.

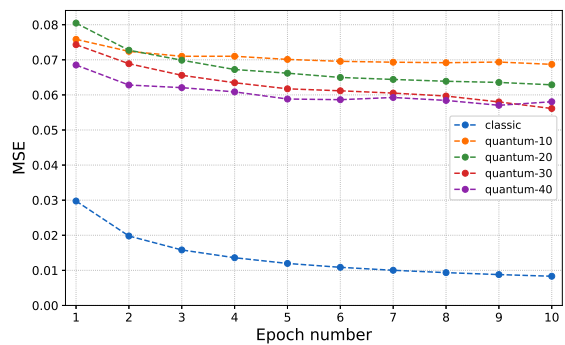
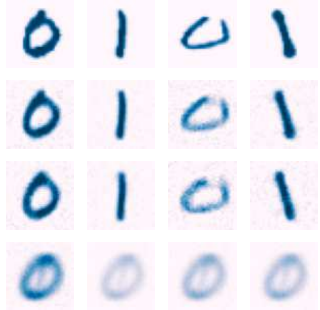


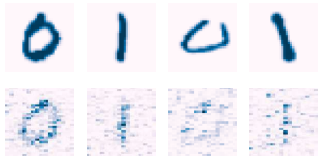
Fig. 5: Validation mean squared error while training various reconstruction neural networks, quantum with different number of layers (10, 20, 30, 40) and classical

We can also look at how the neural network copes with image reconstruction in a more understandable form by comparing the objects of the

experiment we simulated (images from the MNIST dataset) and the images obtained by the neural network, as shown in Fig. 6 and corresponding Structural similarity index metrics (SSIM).



(a) classical with different input layer size



(b) quantum

Fig. 6: Reconstructed images using neural networks trained on the reduced dataset; first row - several images of the reduced MNIST test set; others are images reconstructed by corresponding neural network with 1024 (SSIM = 0.81), 64 (SSIM = 0.76) and 1 (SSIM = 0.18) input layer size respectively for classical one and 64 for quantum (SSIM = 0.25)

For the classical neural network we also got results for the full version of the dataset they are shown in Fig. 7, because it does not take as long as in the quantum case.

6 Conclusion

Classical and quantum neural networks were built to solve problems of classification and reconstruction of images based on the measurements of an object based on the MNIST handwritten digits dataset in the Hadamard basis, which is only 6%

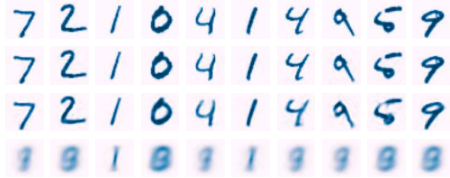


Fig. 7: From top to bottom: (1) several images of the MNIST test set; same ones reconstructed by a classical neural network of (2) 1024 (SSIM = 0.90), (3) 64 (SSIM = 0.86) and (4) 1 (SSIM = 0.18) neurons in the input layer, trained on the entire dataset

of the number of pixels in the original object. The constructed classical classifier showed a prediction accuracy of 96%. The developed classical neural network, which reconstructs an image in a single-pixel detection task, made it possible to obtain a high-quality image with a mean-square error of 0.07 and a structural similarity index of 0.76. It was also investigated how the training quality metrics of the created classical neural networks depend on the number of measurements in the Hadamard basis and it was shown that 64 (6% of all possible) for such a task is the optimal value.

The quantum machine learning method was used to solve the problem of classifying “single-pixel images” and thus demonstrated the applicability of quantum neural networks to the problem of analyzing the problem of single-pixel visualization. A quantum neural network was created and trained on a quantum simulator, which predicts the class of a “single-pixel image” with an accuracy of 95%, which is quite competitive result and could be even better with a number of parameters comparable to the classical case. The quantum neural network for image reconstruction has been developed and the results of its work have been demonstrated; it reconstructs images with a structural similarity index of 0.25. Despite the significant difference from images reconstructed using a classical neural network, this result can also be considered successful as proof of concept for now.

Single-pixel detection is a promising and cost-effective imaging technique across the entire electromagnetic spectrum. Combined with recent

advances in machine learning algorithms, single-pixel detection promises to be a powerful method for low-cost, scan-free 3D recognition and classification, which holds promise for critical applications such as object detection and classification, surface mapping, and 3D situation recognition for autonomous vehicles. And the results obtained in this work give us hope for new and interesting opportunities that quantum machine learning may provide us in the future.

Acknowledgements. We would like to thank the entire team of the MSU.AI project for teaching us a lot and giving many important advices, especially Sergey Kolpinskiy. We also express my deep gratitude to the Laboratory of Experimental and Theoretical Quantum Optics, in particular Dmitry Agapov and Anatoly Chirkin, for productive discussions and valuable comments.

Declarations

Code availability. Source code could be found <https://github.com/Oounce/classical-quantum-mnist.git>.

Conflict of interest. The authors declare that they have no conflict of interest.

Appendix A Quantum computer performance time

To estimate the realistic performance time of a quantum computer, with respect to number of circuits for gradients calculation according to parameter-shift rule [44, 45], we can use the following expression for a single dataset element:

$$t_{el} = (D_{1q} \cdot t_{1q} + D_{2q} \cdot t_{2q}) \cdot (2 \cdot n_{params} + 1) + C,$$

where t_{1q} and t_{2q} are the experimental times of single- and two-qubit gates respectively, $D_{1q(2q)}$ are the circuit depths (maximum number of corresponding gates for one qubit, that can't be parallelized in experiment, which is, with respect to the chosen layer circuit structure (Fig. 3), the sum of number of layers and embedding depth), and C is a constant for setup overheads such as

register initialisation and measurement time and other delays.

Then the total time for one epoch will be:

$$t_{total} = t_{el} \cdot N_{shots} \cdot N_{dataset},$$

where N_{shots} is number of each quantum circuit runs to get statistics for the expected value, $N_{dataset}$ is number of elements in dataset.

References

- [1] Gibson, G.M., Johnson, S.D., Padgett, M.J.: Single-pixel imaging 12 years on: a review. *Optics express* **28**(19), 28190–28208 (2020) <https://doi.org/10.1364/OE.403195>
- [2] Biamonte, J., Wittek, P., Pancotti, N., Rebentrost, P., Wiebe, N., Lloyd, S.: Quantum machine learning. *Nature* **549**(7671), 195–202 (2017) <https://doi.org/10.1038/nature23474>
- [3] Schuld, M., Sinayskiy, I., Petruccione, F.: An introduction to quantum machine learning. *Contemporary Physics* **56**(2), 172–185 (2015) <https://doi.org/10.1080/00107514.2014.964942>
- [4] Ciliberto, C., Herbster, M., Ialongo, A.D., Pontil, M., Rocchetto, A., Severini, S., Wossnig, L.: Quantum machine learning: a classical perspective. *Proceedings of the Royal Society A: Mathematical, Physical and Engineering Sciences* **474**(2209), 20170551 (2018) <https://doi.org/10.1098/rspa.2017.0551>
- [5] Benedetti, M., Lloyd, E., Sack, S., Fiorentini, M.: Parameterized quantum circuits as machine learning models. *Quantum Science and Technology* **4**(4), 043001 (2019) <https://doi.org/10.1088/2058-9565/ab4eb5>
- [6] Nielsen, M.A., Chuang, I.L.: *Quantum Computation and Quantum Information*. Cambridge university press, Cambridge (2010)
- [7] Cerezo, M., Arrasmith, A., Babbush, R., Benjamin, S.C., Endo, S., Fujii, K., McClean, J.R., Mitarai, K., Yuan, X., Cincio, L., *et al.*: Variational quantum algorithms. *Nature Reviews Physics* **3**(9), 625–644

- (2021) <https://doi.org/10.1038/s42254-021-00348-9>
- [8] Sharma, K., Khatri, S., Cerezo, M., Coles, P.J.: Noise resilience of variational quantum compiling. *New Journal of Physics* **22**(4), 043006 (2020) <https://doi.org/10.1088/1367-2630/ab784c>
- [9] Phillipson, F.: Quantum computing in logistics and supply chain management-an overview. arXiv preprint arXiv:2402.17520 (2024) <https://doi.org/10.48550/arXiv.2402.17520>
- [10] Herman, D., Googin, C., Liu, X., Sun, Y., Galda, A., Safro, I., Pistoia, M., Alexeev, Y.: Quantum computing for finance. *Nature Reviews Physics* **5**(8), 450–465 (2023) <https://doi.org/10.1038/s42254-023-00603-1>
- [11] Ur Rasool, R., Ahmad, H.F., Rafique, W., Qayyum, A., Qadir, J., Anwar, Z.: Quantum computing for healthcare: A review. *Future Internet* **15**(3), 94 (2023) <https://doi.org/10.3390/fi15030094>
- [12] Liu, J.: Towards real-world implementations of quantum machine learning. *Quantum Views* **7**, 77 (2023)
- [13] Dilmegani, C.: Top 20 Quantum Computing Use Cases & Applications in 2024. <https://research.aimultiple.com/quantum-computing-applications/>
- [14] Greenberg, J., Krishnamurthy, K., Brady, D.: Compressive single-pixel snapshot x-ray diffraction imaging. *Optics letters* **39**(1), 111–114 (2014) <https://doi.org/10.1364/OL.39.000111>
- [15] Yu, H., Lu, R., Han, S., Xie, H., Du, G., Xiao, T., Zhu, D.: Fourier-transform ghost imaging with hard x rays. *Physical review letters* **117**(11), 113901 (2016) <https://doi.org/10.1103/PhysRevLett.117.113901>
- [16] Zhang, A.-X., He, Y.-H., Wu, L.-A., Chen, L.-M., Wang, B.-B.: Tabletop x-ray ghost imaging with ultra-low radiation. *Optica* **5**(4), 374–377 (2018) <https://doi.org/10.1364/OPTICA.5.000374>
- [17] Chan, W.L., Charan, K., Takhar, D., Kelly, K.F., Baraniuk, R.G., Mittleman, D.M.: A single-pixel terahertz imaging system based on compressed sensing. *Applied Physics Letters* **93**(12) (2008) <https://doi.org/10.1063/1.2989126>
- [18] Shrekenhamer, D., Watts, C.M., Padilla, W.J.: Terahertz single pixel imaging with an optically controlled dynamic spatial light modulator. *Optics express* **21**(10), 12507–12518 (2013) <https://doi.org/10.1364/OE.21.012507>
- [19] Stantchev, R.I., Yu, X., Blu, T., Pickwell-MacPherson, E.: Real-time terahertz imaging with a single-pixel detector. *Nature communications* **11**(1), 2535 (2020) <https://doi.org/10.1038/s41467-020-16370-x>
- [20] Edgar, M.P., Gibson, G.M., Bowman, R.W., Sun, B., Radwell, N., Mitchell, K.J., Welsh, S.S., Padgett, M.J.: Simultaneous real-time visible and infrared video with single-pixel detectors. *Scientific reports* **5**(1), 10669 (2015) <https://doi.org/10.1038/srep10669>
- [21] Osorio Quero, C., Durini, D., Rangel-Magdaleno, J., Martinez-Carranza, J., Ramos-Garcia, R.: Single-pixel near-infrared 3d image reconstruction in outdoor conditions. *Micromachines* **13**(5), 795 (2022) <https://doi.org/10.3390/mi13050795>
- [22] Gibson, G.M., Sun, B., Edgar, M.P., Phillips, D.B., Hempler, N., Maker, G.T., Malcolm, G.P., Padgett, M.J.: Real-time imaging of methane gas leaks using a single-pixel camera. *Optics express* **25**(4), 2998–3005 (2017) <https://doi.org/10.1364/OE.25.002998>
- [23] Candès, E.J., Wakin, M.B.: An introduction to compressive sampling. *IEEE signal processing magazine* **25**(2), 21–30 (2008)
- [24] Katz, O., Bromberg, Y., Silberberg, Y.: Compressive ghost imaging. *Applied Physics Letters* **95**(13) (2009) <https://doi.org/10.1063/1.3238296>

- [25] Davenport, M.A., Boufounos, P.T., Wakin, M.B., Baraniuk, R.G.: Signal processing with compressive measurements. *IEEE Journal of Selected topics in Signal processing* **4**(2), 445–460 (2010) <https://doi.org/10.1109/JSTSP.2009.2039178>
- [26] Higham, C.F., Murray-Smith, R., Padgett, M.J., Edgar, M.P.: Deep learning for real-time single-pixel video. *Scientific reports* **8**(1), 2369 (2018) <https://doi.org/10.1038/s41598-018-20521-y>
- [27] Radwell, N., Johnson, S.D., Edgar, M.P., Higham, C.F., Murray-Smith, R., Padgett, M.J.: Deep learning optimized single-pixel lidar. *Applied Physics Letters* **115**(23) (2019) <https://doi.org/10.1063/1.5128621>
- [28] Zhang, Z., Li, X., Zheng, S., Yao, M., Zheng, G., Zhong, J.: Image-free classification of fast-moving objects using “learned” structured illumination and single-pixel detection. *Optics express* **28**(9), 13269–13278 (2020) <https://doi.org/10.1364/OE.392370>
- [29] Jiao, S., Feng, J., Gao, Y., Lei, T., Xie, Z., Yuan, X.: Optical machine learning with incoherent light and a single-pixel detector. *Optics letters* **44**(21), 5186–5189 (2019)
- [30] Zaidenberg, D.A., Sebastianelli, A., Spiller, D., Le Saux, B., Ullo, S.L.: Advantages and bottlenecks of quantum machine learning for remote sensing. In: 2021 IEEE International Geoscience and Remote Sensing Symposium IGARSS, pp. 5680–5683 (2021). <https://doi.org/10.1109/IGARSS47720.2021.9553133>. IEEE
- [31] Adhikary, S., Dangwal, S., Bhowmik, D.: Supervised learning with a quantum classifier using multi-level systems. *Quantum Information Processing* **19**, 1–12 (2020) <https://doi.org/10.1007/s11128-020-2587-9>
- [32] McClean, J.R., Boixo, S., Smelyanskiy, V.N., Babbush, R., Neven, H.: Barren plateaus in quantum neural network training landscapes. *Nature communications* **9**(1), 4812 (2018) <https://doi.org/10.1038/s41467-018-07090-4>
- [33] Arrasmith, A., Cerezo, M., Czarnik, P., Cincio, L., Coles, P.J.: Effect of barren plateaus on gradient-free optimization. *Quantum* **5**, 558 (2021) <https://doi.org/10.22331/q-2021-10-05-558>
- [34] Pesah, A., Cerezo, M., Wang, S., Volkoff, T., Sornborger, A.T., Coles, P.J.: Absence of barren plateaus in quantum convolutional neural networks. *Physical Review X* **11**(4), 041011 (2021) <https://doi.org/10.1103/PhysRevX.11.041011>
- [35] Hur, T., Kim, L., Park, D.K.: Quantum convolutional neural network for classical data classification. *Quantum Machine Intelligence* **4**(1), 3 (2022) <https://doi.org/10.1007/s42484-021-00061-x>
- [36] Liu, J., Lim, K.H., Wood, K.L., Huang, W., Guo, C., Huang, H.-L.: Hybrid quantum-classical convolutional neural networks. *Science China Physics, Mechanics & Astronomy* **64**(9), 290311 (2021) <https://doi.org/10.1007/s11433-021-1734-3>
- [37] Li, W., Chu, P.-C., Liu, G.-Z., Tian, Y.-B., Qiu, T.-H., Wang, S.-M.: An image classification algorithm based on hybrid quantum classical convolutional neural network. *Quantum Engineering* **2022**(1), 5701479 (2022) <https://doi.org/10.1155/2022/5701479>
- [38] Senokosov, A., Sedykh, A., Saginalieva, A., Kyriacou, B., Melnikov, A.: Quantum machine learning for image classification. *Machine Learning: Science and Technology* **5**(1), 015040 (2024) <https://doi.org/https://doi.org/10.1088/2632-2153/ad2aef>
- [39] Huang, H.-L., Du, Y., Gong, M., Zhao, Y., Wu, Y., Wang, C., Li, S., Liang, F., Lin, J., Xu, Y., *et al.*: Experimental quantum generative adversarial networks for image generation. *Physical Review Applied* **16**(2), 024051 (2021) <https://doi.org/10.1103/PhysRevApplied.16.024051>
- [40] Rudolph, M.S., Toussaint, N.B., Katarbarwa, A., Johri, S., Peropadre, B., Perdomo-Ortiz, A.: Generation of high-resolution handwritten digits with an ion-trap quantum

computer. *Physical Review X* **12**(3), 031010 (2022) <https://doi.org/10.1103/PhysRevX.12.031010>

- [41] Park, D.K., Petruccione, F., Rhee, J.-K.K.: Circuit-based quantum random access memory for classical data. *Scientific reports* **9**(1), 3949 (2019) <https://doi.org/10.1038/s41598-019-40439-3>
- [42] Larocca, M., Ju, N., García-Martín, D., Coles, P.J., Cerezo, M.: Theory of overparametrization in quantum neural networks. *Nature Computational Science* **3**(6), 542–551 (2023) <https://doi.org/10.1038/s43588-023-00467-6>
- [43] Georgescu, I.M., Ashhab, S., Nori, F.: Quantum simulation. *Reviews of Modern Physics* **86**(1), 153–185 (2014) <https://doi.org/10.1103/RevModPhys.86.153>
- [44] Mitarai, K., Negoro, M., Kitagawa, M., Fujii, K.: Quantum circuit learning. *Physical Review A* **98**(3), 032309 (2018) <https://doi.org/10.1103/PhysRevA.98.032309>
- [45] Schuld, M., Bergholm, V., Gogolin, C., Izaac, J., Killoran, N.: Evaluating analytic gradients on quantum hardware. *Physical Review A* **99**(3), 032331 (2019) <https://doi.org/10.1103/PhysRevA.99.032331>